NAVAL POSTGRADUATE SCHOOL
MONTEREY, CALIFORNIA

THESIS

A SIMULATION STUDY OF THE
VARIABILITY OF
ACOUSTIC TRANSMISSIONS
FROM HAWAII TO MONTEREY

by

Robert A. Staten

September, 1995

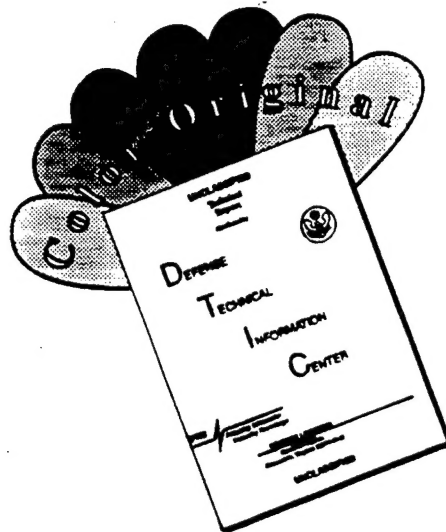| Thesis Advisors: | Ching-Sang Chiu |
| | Albert J. Semtner |

Approved for public release; distribution is unlimited.

19960501 182   DTIC QUALITY INSPECTED 1

DISCLAIMER NOTICE

THIS DOCUMENT IS BEST QUALITY AVAILABLE. THE COPY FURNISHED TO DTIC CONTAINED A SIGNIFICANT NUMBER OF COLOR PAGES WHICH DO NOT REPRODUCE LEGIBLY ON BLACK AND WHITE MICROFICHE.

REPORT DOCUMENTATION PAGE

Form Approved OMB No. 0704-0188

Public reporting burden for this collection of information is estimated to average 1 hour per response, including the time for reviewing instruction, searching existing data sources, gathering and maintaining the data needed, and completing and reviewing the collection of information. Send comments regarding this burden estimate or any other aspect of this collection of information, including suggestions for reducing this burden, to Washington Headquarters Services, Directorate for Information Operations and Reports, 1215 Jefferson Davis Highway, Suite 1204, Arlington, VA 22202-4302, and to the Office of Management and Budget, Paperwork Reduction Project (0704-0188) Washington DC 20503.

1. AGENCY USE ONLY (Leave blank)	2. REPORT DATE September 1995	3. REPORT TYPE AND DATES COVERED Master's Thesis

4. TITLE AND SUBTITLE A SIMULATION STUDY OF THE VARIABILITY OF ACOUSTIC TRANSMISSIONS FROM HAWAII TO MONTEREY	5. FUNDING NUMBERS
6. AUTHOR(S) Robert A. Staten	

7. PERFORMING ORGANIZATION NAME(S) AND ADDRESS(ES) Naval Postgraduate School Monterey CA 93943-5000	8. PERFORMING ORGANIZATION REPORT NUMBER

9. SPONSORING/MONITORING AGENCY NAME(S) AND ADDRESS(ES) Acoustic Thermometry of Ocean Climate Project Scripps Institution of Oceanography 9500 Gilman Drive, 0225 La Jolla, CA 92093-0225	10. SPONSORING/MONITORING AGENCY REPORT NUMBER

11. SUPPLEMENTARY NOTES The views expressed in this thesis are those of the author and do not reflect the official policy or position of the Department of Defense or the U.S. Government.

12a. DISTRIBUTION/AVAILABILITY STATEMENT Approved for public release; distribution is unlimited.	12b. DISTRIBUTION CODE

13. ABSTRACT (maximum 200 words)

As part of the modeling effort in the Acoustic Thermometry of Ocean Climate (ATOC) project, the influence of mesoscale, gyrescale and seasonal ocean variability on three-dimensional (3D) acoustic ray paths from the planned Hawaii to Monterey site is investigated. Ray paths and signal arrival structure over a two year period are simulated at a six-day interval using a 3D ray-based acoustic model. The input sound speed fields are interpolated from gridded (1/4 degree, 20 level) temperature and salinity output data from the Semtner-Chervin eddy-resolving Parallel Ocean Climate Model. Based on the simulated acoustic multipath arrival structure, the issues of stability and travel time variability are addressed. Bottom topography in the Moonless Mountains region is found to have occasional mild effects on steeper rays. Arrival structure is found to be strongly dependent on depth and quasi-stable over time with a 0.6 correlation between arrival patterns at different times. Travel time variability estimates are 0.42 s rms for steep rays, due to a combination of seasonal and mesoscale ocean variability, and 0.28 s rms for near-axial rays, due primarily to seasonal variability.

14. SUBJECT TERMS Ocean Acoustics, Acoustic Model, Oceanography, ATOC, Acoustic Thermometry of Ocean Climate	15. NUMBER OF PAGES 50
	16. PRICE CODE

17. SECURITY CLASSIFICATION OF REPORT Unclassified	18. SECURITY CLASSIFICATION OF THIS PAGE Unclassified	19. SECURITY CLASSIFICATION OF ABSTRACT Unclassified	20. LIMITATION OF ABSTRACT UL

NSN 7540-01-280-5500

Standard Form 298 (Rev. 2-89)
Prescribed by ANSI Std. 239-18 298-102

i

A SIMULATION STUDY OF THE VARIABILITY
OF ACOUSTIC TRANSMISSIONS
FROM HAWAII TO MONTEREY

Robert A. Staten

Lieutenant, United States Navy

B.S., United States Naval Academy, 1988

Submitted in partial fulfillment

of the requirements for the degree of

MASTER OF SCIENCE IN PHYSICAL OCEANOGRAPHY

from the

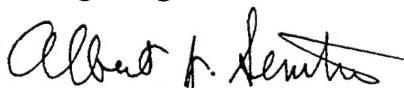**NAVAL POSTGRADUATE SCHOOL**
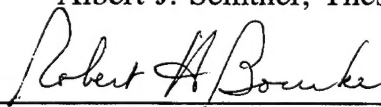**September 1995**

Author: _____

Robert A. Staten

Approved by: _____

Ching-Sang Chiu, Thesis Advisor

_____

Albert J. Semtner, Thesis Co-Advisor

_____

Robert H. Bourke, Chairman
Department of Oceanography

iii

ABSTRACT

As part of the modeling effort in the Acoustic Thermometry of Ocean Climate (ATOC) project, the influence of mesoscale, gyrescale and seasonal ocean variability on three-dimensional (3D) acoustic ray paths from the planned Hawaii to Monterey site is investigated. Ray paths and signal arrival structure over a two year period are simulated at a six-day interval using a 3D ray-based acoustic model. The input sound speed fields are interpolated from gridded (1/4 degree, 20 level) temperature and salinity output data from the Semtner-Chervin eddy-resolving Parallel Ocean Climate Model. Based on the simulated acoustic multipath arrival structure, the issues of stability and travel time variability are addressed. Bottom topography in the Moonless Mountains region is found to have occasional mild effects on steeper rays. Arrival structure is found to be strongly dependent on depth and quasi-stable over time with a 0.6 correlation between arrival patterns at different times. Travel time variability estimates are 0.42 s rms for steep rays, due to a combination of seasonal and mesoscale ocean variability, and 0.28 s rms for near-axial rays, due primarily to seasonal variability.

TABLE OF CONTENTS

ACKNOWLEDGEMENTS

x

I. INTRODUCTION

A. ACOUSTIC THERMOMETRY OF OCEAN CLIMATE

We have observed the concentrations of "greenhouse gases" increasing at a significant rate, yet debate still exists over several key issues:

1.   the amount of global warming that will result from the build-up of these gases,

2.   the length of time over which global warming will take place, and

3.   the discernability and predictability of warming trends, given our current data, networks and models.

Difficulties arise in trying to determine warming trends from atmospheric measurements, as they have similar spatial patterns to the background air temperature variability.   In addition, many land stations are contaminated by the "urban heat-center" effect and are further biased by the northerly distribution of most observation stations (Munk and Forbes, 1989).

Munk and Forbes proposed "Underwater Acoustic Thermometry" in 1989 as a method for the early detection of global warming.   Using a network of projectors and receivers distributed worldwide, acoustic signal travel time variability would be measured over a ten year period and theoretically yield a quantitative estimate of global warming.   An advantage to utilizing the ocean rather than the atmosphere to detect

warming trends is that the warming signal is significantly different than the pattern of inherent variability of the ocean (Munk and Forbes, 1989).

In 1991 the Heard Island Feasibility Test (HIFT) sought to answer questions concerning transmission and reception of trans-global acoustic signals. Coded acoustic transmissions originating from Heard Island in the southern Indian Ocean were monitored at 16 sites in the Atlantic, Pacific, Indian, and Southern Oceans. The successful test established that low-frequency sound from modulated sources could be transmitted reliably over great distances with sufficient intensity.

The effects of background ocean variability on acoustic variability for the Heard-to-California path was studied by Chiu *et al.* (1994) utilizing a similar global ocean circulation model to that used for this study. An important conclusion was that excessive background travel time fluctuation of 2.5 s rms would preclude detection of the greenhouse signal in ten years along this 18-megameter path, since the rate of travel time increase due to potential warming was estimated by Munk and Forbes (1989) to be 1 s per decade along trans-global paths. This significant travel time fluctuation was caused by the highly variable Antarctic Circumpolar Front, through which the Heard-to-California path traversed.

The HIFT was prerequisite to the current Scripps

2

Institution of Oceanography's program, Acoustic Thermometry of Ocean Climate (ATOC). Avoiding transmissions through the Antarctic Polar Front, ATOC calls for a planned network of sites located throughout the Pacific, including two acoustic sources to be deployed near California and Hawaii. Receiver sites include existing U.S. Navy facilities, several fixed Vertical Line Arrays (VLA's), and drifting Surface Suspended Acoustic Receivers (SSAR's). Figure 1 shows what the planned network looks like.

In addition to measuring ocean climate change, another benefit of a cross-basin acoustic thermometry system would be enhancement of ocean nowcast/forecast capability. Basin specific information on gyre scale and mesoscale processes could be obtained by travel time fluctuations along paths through specific basins. Travel time variability information can be used to validate/calibrate ocean nowcast/forecast models.

B.   ACOUSTIC ISSUES

There are three acoustic issues that are of great concern to and must be addressed by ATOC. The first is acoustic reliability. It must be known whether a site will be ensonified all year round. The location of the sound source determines locations of ensonified and shadow zones. These zones fluctuate as a function of time due to the variability of the ocean.
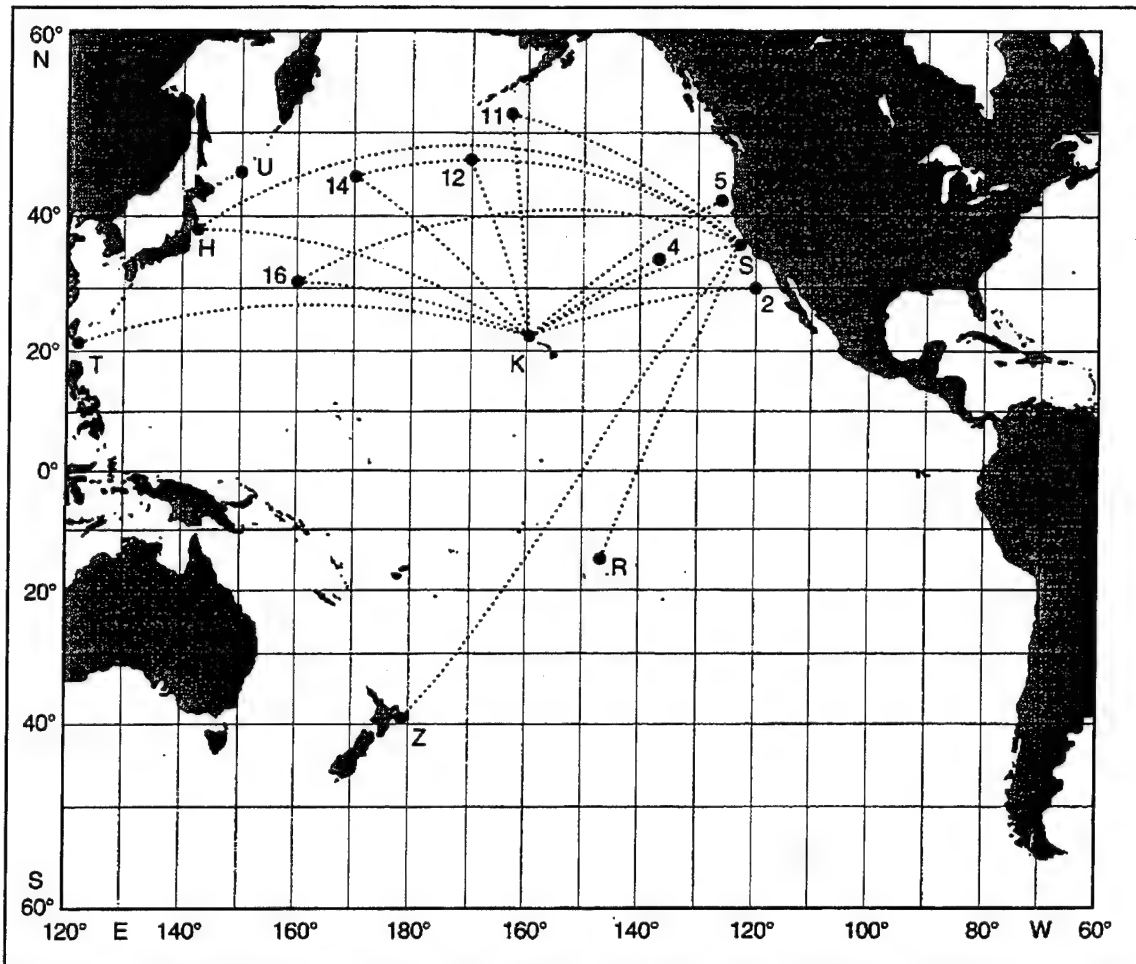
Figure 1. Proposed site locations for ATOC project. The nominal positions (as of the beginning of this study) of the two planned sources are shown near Kauai (K) and Point Sur (S), with a variety of receivers denoted by other letters and numbers (Cartwright, 1993)

The next issue is acoustic stability. It must be determined whether significant portions of the acoustic arrival patterns change over an extended period of time. Only stable arrivals can be used to construct useful travel-time series.

The final issue deals with geophysical noise. Frontal effects, mesoscale eddies and seasonal cycles cause travel time fluctuations that can be interpreted as "noise" relative

4

to the greenhouse signal. The size of these fluctuations dictates the length of observation needed before a statistically significant trend can be revealed. Different acoustic paths traverse different ocean features of varying strengths. Consequently, arrival time fluctuations vary from location to location. The most ideal receiving locations are those which are reliable, with stable arrivals, and those having minimal geophysical noise in the travel times.

C.   THESIS OBJECTIVES AND APPROACH

This thesis focuses on the Hawaii-to-California path, examining the effects of seasonal and mesoscale variability and single-phone arrival structure. Issues of acoustic reliability and stability are addressed and travel time variability is quantified.

The analysis of acoustic variability was conducted by interfacing an acoustic model with a circulation model. A three-dimensional raytracing computer program called the Hamiltonian Acoustic Raytracing Program for the Ocean (HARPO) was used for the acoustic model. The Semtner-Chervin Parallel Ocean Climate Model (POCM) served as the ocean circulation model, providing simulated salinity and temperature fields. HARPO requires a continuous sound-speed field as input and an interpolation procedure was used to interface HARPO with the ocean model. Fans of acoustic rays and the corresponding parameters were computed for every six days in a two year model period. For every six-day "ocean snapshot" eigenrays

5

were identified and arrival structures were constructed.

Time series of arrival structure for two different receiver depths were analyzed. The depth of 700m corresponds to the approximate depth of the sound channel axis off the coast of California, and the 1359m depth corresponds to the approximate depth of a single hydrophone of an existing array located near Point Sur.

D.   THESIS OUTLINE

The remainder of this thesis consists of three chapters. Chapter II contains a description of the approach, including brief descriptions of HARPO, the Semtner-Chervin model, and the acoustics-ocean interface procedure. Also included is a description of the arrival structure generation procedure. In Chapter III, results are presented and analyzed. Chapter IV presents the conclusions and recommendations of this thesis.

II. DESCRIPTION OF APPROACH

A. HAMILTONIAN ACOUSTIC RAYTRACING

The acoustic model used to trace raypaths is the Hamiltonian Acoustic Raytracing Program for the Ocean (HARPO). Originating from NOAA (Jones *et al.*, 1986), HARPO is a computer program that numerically integrates Hamilton's equations of motion in spherical polar coordinates for three-dimensional acoustic ray paths through a model ocean. The input ocean model is required to have a continuous three-dimensional sound speed field with a continuous representation of both the sea surface and bathymetry. An updated version of HARPO that contains an interpolating interface to gridded data (Chiu *et al.*, 1994) was used for this study to perform all raytracing on a workstation.

The initial conditions for the integrations consist of vertical and azimuthal launch angles of the rays. The effect of the Earth's curvature is accounted for since HARPO performs calculations in polar coordinates, but geodesic veering due to the elliptical shape of the Earth is not accounted for.

B. OCEAN MODEL

The ocean environment model used is the Semtner-Chervin Parallel Ocean Climate Model (POCM) (Semtner, 1995), a descendent of the eddy-resolving Semtner-Chervin Global Ocean Circulation Model (SCGCM) (Semtner and Chervin, 1988 and 1992). Improvements can be attributed in part to the model's

7

ability to harness the parallel processors of the CRAY Y-MP/8 supercomputer at the National Center for Atmospheric Research (NCAR). The model is gridded with 1/4° average horizontal resolution and has a domain extending from 75°S to 65°N. In the vertical plane there are 20 levels with an approximate resolution of 25 m in the upper 100 m, with decreasing resolution with increasing depth. Model ocean depths were obtained from NCAR for 1/12° latitude and longitude points and averaged to correspond to local model resolution. Coastlines were also prescribed at the local model resolution and not smoothed and simplified as in the earlier model.

The uppermost levels are forced on a monthly basis to values from the Levitus climatological data set. Momentum fluxes are derived from smoothly interpolated monthly values of European Center for Medium Range Weather Forecasting (ECMWF) wind stress at 1000 mb for the period of 1985-1989. Subsurface restoring of temperature and salinity is only used north of 58°S, south of 68°N, and in the vicinity of Gibraltar.

Initialization of the model was accomplished by using the full 33 year spin-up of the SCGCM to generate instantaneous fields, which were then interpolated to the 1/4° grid spacing. The model was resumed, starting with the ECMWF winds of 1985. At the end of each 3-day period, a "snapshot" was taken of the global ocean and archived at NCAR. For this thesis every other archived data set was used for years 1987 and 1988

8

resulting in a six-day resolution over a period of two years.

C.   OCEAN-ACOUSTIC INTERFACE

HARPO requires continuous data fields as its input for computations.   An earlier procedure to interface HARPO to gridded ocean model data (Newhall *et al.*, 1990) was modified by Chiu *et al.* in 1994 and used for this interface.   This method makes computations possible on local workstations with limited hard disk space and memory.   Since the global data sets archived at NCAR are very large, it was desirable to subsample only the data pertaining to our region of interest.

Temperature, salinity, and bathymetry data were extracted for the specific region from the global data set.   Sound speed was then calculated from temperature and salinity data using the Mackenzie empirical formula (Mackenzie, 1981).   To limit the computational demand, a 5° by 5° window was used to move along with the traced ray.   Inside of the window sound speed was expressed as a sum of the mean speed and perturbed speed. The perturbation was further expressed as a linear combination of empirical orthogonal functions (EOF's).   All perturbation EOF's, mean profiles, and bathymetry data were splined to produce smooth and continuous input fields for HARPO.   After each ray was traced to a point near the edge of the window, the window was shifted to center at that point and new sound speed and bathymetry data were subsampled and processed, and raytracing continued.

D. MULTIPATH ARRIVAL STRUCTURE GENERATION

HARPO does not perform eigenray searches and compute signal amplitudes and phase shifts. An external MATLAB™ program called *ray3d.m* (Chiu, 1995) was used to perform these functions based on the HARPO outputs. The program first determines the location where each wavefront (i.e., surface normal to a ray) intercepts the receiver as a function of launch angle by using a local tangent-normal analysis. As sketched in Figure 2, HARPO outputs the position vectors as well as local ray angles of points along each traced ray (i.e., ray points). These HARPO outputs are used to calculate
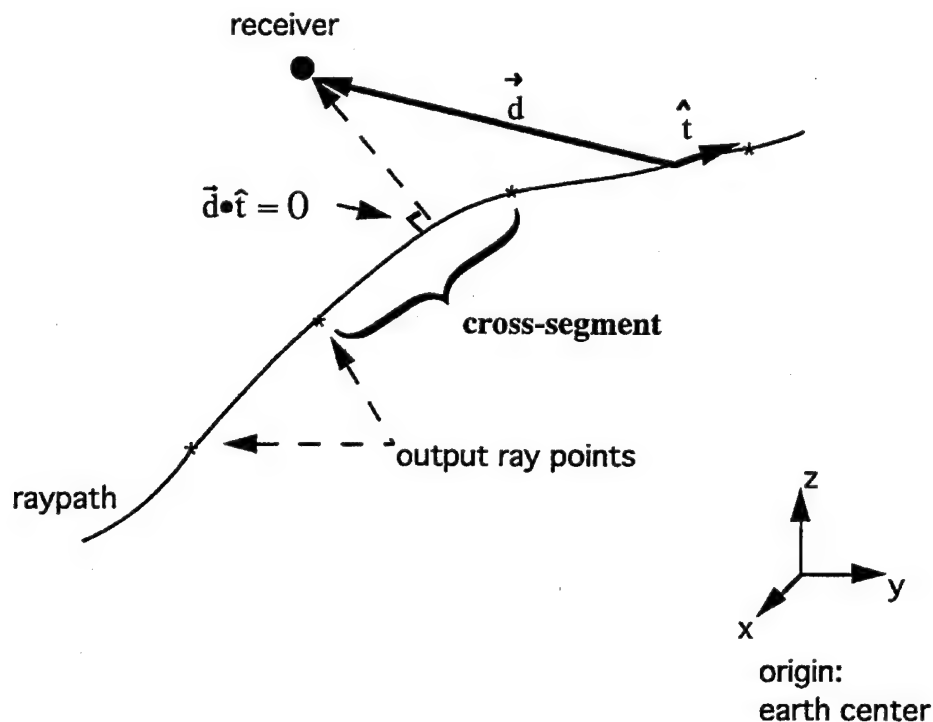

Figure 2. Determination of the position along a ray where the corresponding wavefront crosses the receiver using a local tangent-normal coordinate analysis. $\vec{d}$ is a displacement vector defining the distance and direction from any position on the ray to the receiver and $\hat{t}$ is a tangent directional vector along the ray.

10

displacement vectors $\vec{d}$ pointing to the receiver and unit directional vectors t tangent to the ray at those ray points. As the wavefront of the ray crosses the receiver, a sign change in $\vec{d} \cdot t$ occurs and thus the "cross-segment" is determined. The exact interception point within the ray cross-segment is found by fitting a polynomial to the positions and ray angles of the two local ray points and then solving for $\vec{d} \cdot t = 0$.

Based on the calculated interception points of the traced ray fan, a depth-versus-launch elevation angle curve can be constructed. As shown in Figure 3, the points where such a curve intersects the receiver depth line gives the launch angles of the eigenrays. For these intersection points, eigenray parameters are interpolated for, including initial angles, arrival times, number of turning points, etc.

Eigenrays with five or more bottom or surface interactions are not included and would not be considered reliable ray paths. For each individual eigenray arrival, spreading loss, boundary loss and phase changes are accounted for. Then the time-translated, phase-shifted and amplitude-modified signal arrivals are coherently summed.
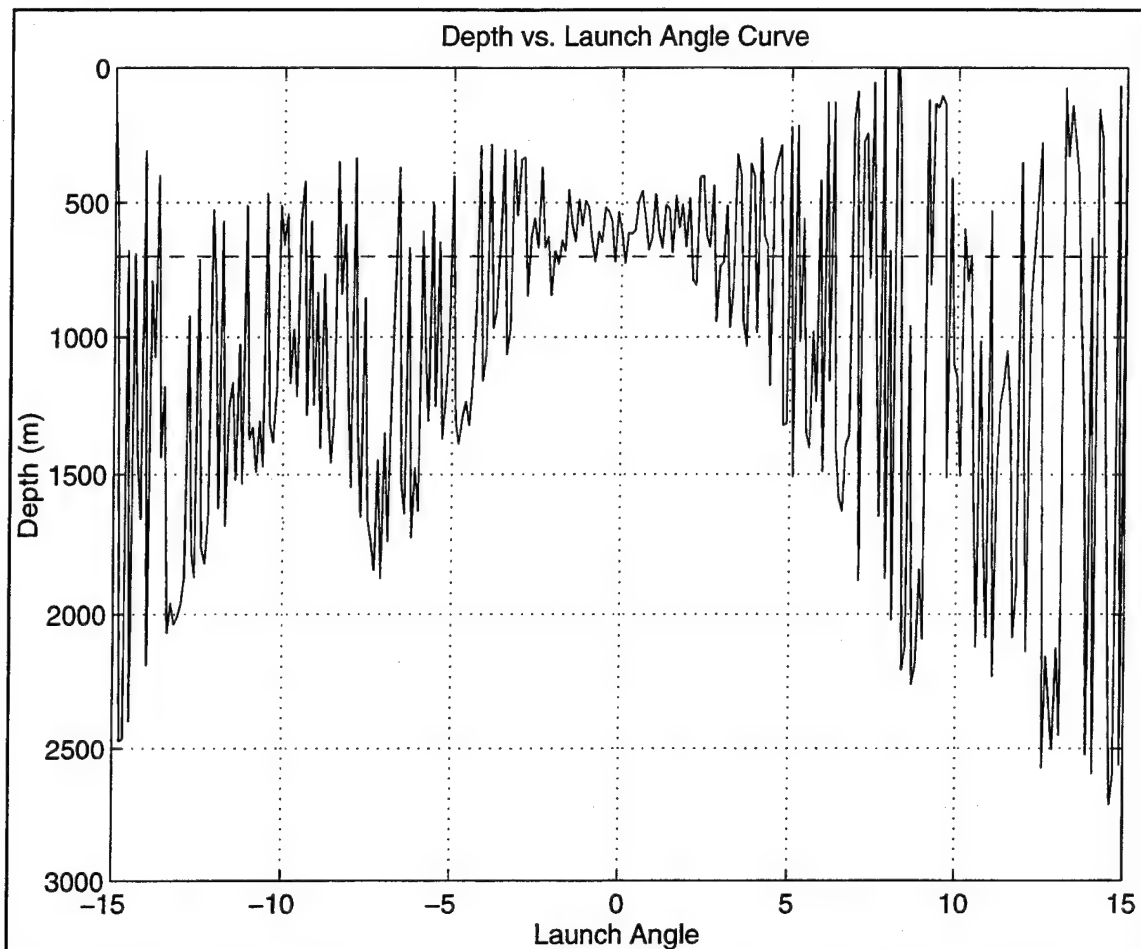
Figure 3. Typical depth-versus-launch elevation angle curve (solid line). A receiver depth at 700 m is also plotted (dashed line). The intersections give the launch elevation angles of the eigenrays.

III. ANALYSIS AND RESULTS

A. ENVIRONMENT

1. Fronts/Circulation

The general pattern of circulation in the North Pacific has a concentrated north-eastward current flow in the western half with a widely dispersed southern return flow in the eastern half. The most notable circulation feature is the sub-tropical front, a region of convergence located just north of Hawaii and stretching east-west in direction. In this region warmer surface water tends to be forced downward by the converging circulation at the center of the Pacific gyre. This feature is well represented in the Semtner-Chervin POCM and can be observed in both the horizontal and vertical slices of the sound speed fields (to be displayed in upcoming figures). The deep sound channel axis does not vary a great deal, ranging from 850 m near Hawaii to about 700 m near the coast of California.

2. Bathymetry

In comparison to other parts of the Pacific basin the topography of the northeastern region tends to be somewhat smooth; however, sections underlying the transmission paths can occasionally provide an obstacle (i.e., a complication) to some steeper acoustic rays.

Several fracture zones cover the eastern Pacific basin and they are characterized by extremely rough and elevated
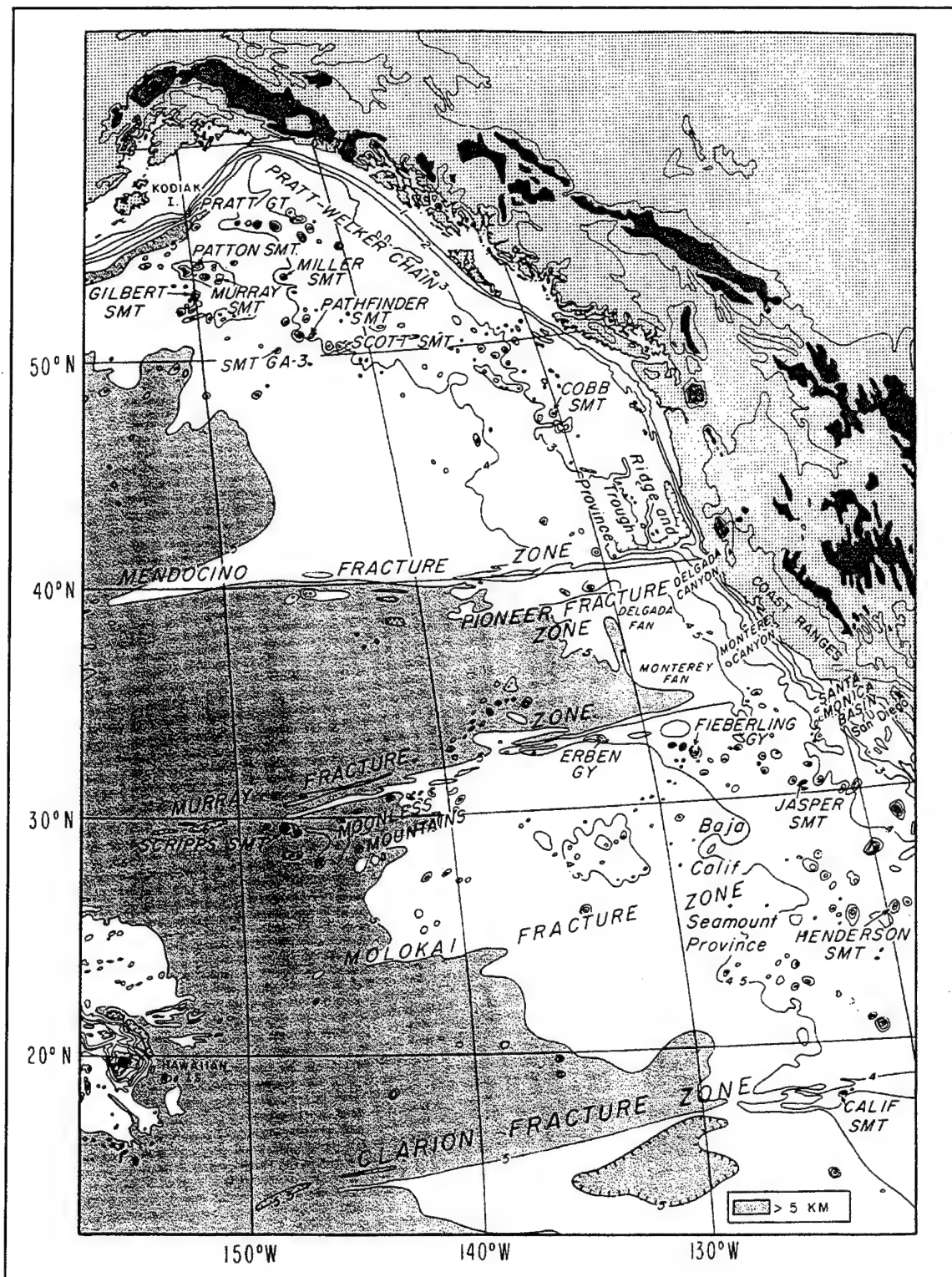
Figure 4. Bathymetry of the Pacific Basin (Menard, 1964).

14

terrain relative to the surrounding area. As can be seen in Figure 4, the Murray Fracture Zone stretches east-west for several thousand kilometers, crossing the trajectory of the raypaths approximately half way. In this particular region the Moonless Mountains rise to within nearly 2000 m of the sea surface, thereby affecting in some way deeper cycling raypaths.

B.   OCEAN MODEL VARIABILITY

1.   Spatial Variability

Figure 5 displays a horizontal section of an instantaneous sound speed field simulated by the POCM at a depth of 435 m. Substantial horizontal variability exists between Hawaii and California at this level, and approximate locations of significant mesoscale features including the subtropical front can be discerned. In contrast, Figure 6 displays sound speed at 847 m, with noticeably reduced variability (note color axis scaling).

Figure 7 presents a vertical slice of an instantaneous sound speed field along a path between the source and the receivers. Vertical gradients in sound speed are significant in the upper 500 m of the water column, especially in the vicinity of the subtropical front. Below 500 m changes are relatively gradual. A three-dimensional view of the complex input bathymetry is shown in Figure 8. A near-axial cycling raypath is superimposed on the figure as well as the source and receiver locations.
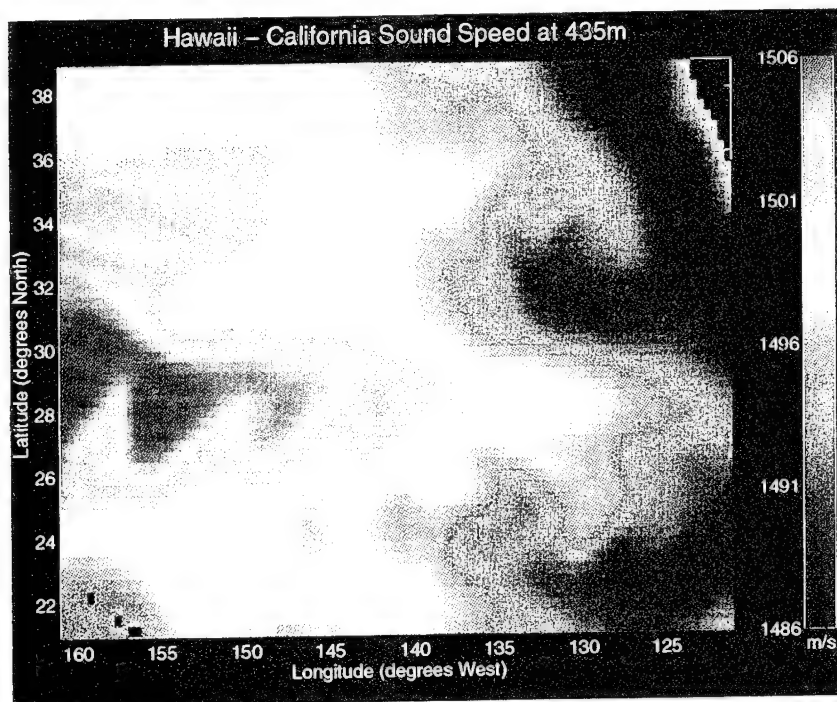
15

Figure 5. Horizontal layer of sound speed at a depth of 435 m between Hawaii and California, a snapshot.
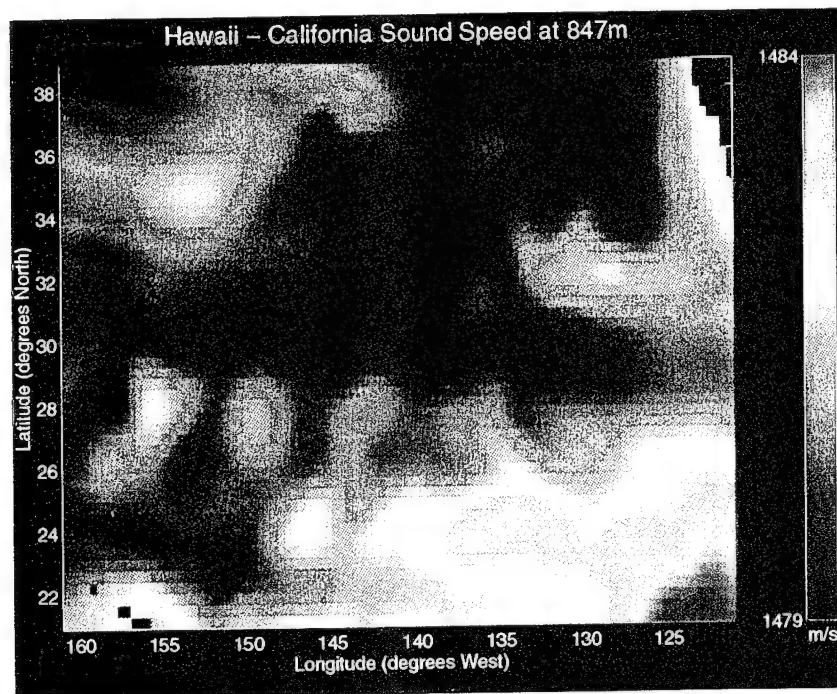

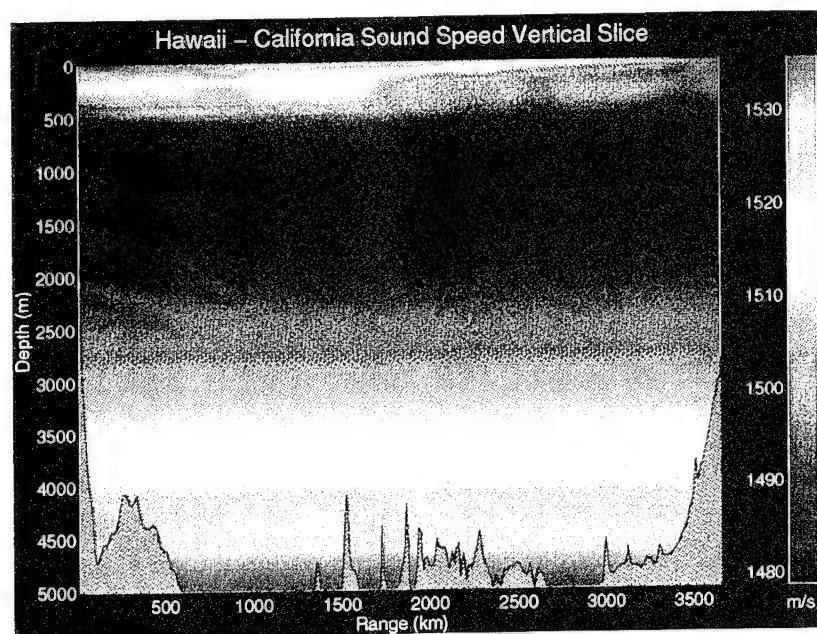**Figure 6.** Horizontal layer of sound speed at a depth of 847 m between Hawaii and California, a snapshot.

16

Figure 7. Vertical slice of sound speed field between Hawaii and California, a snapshot.
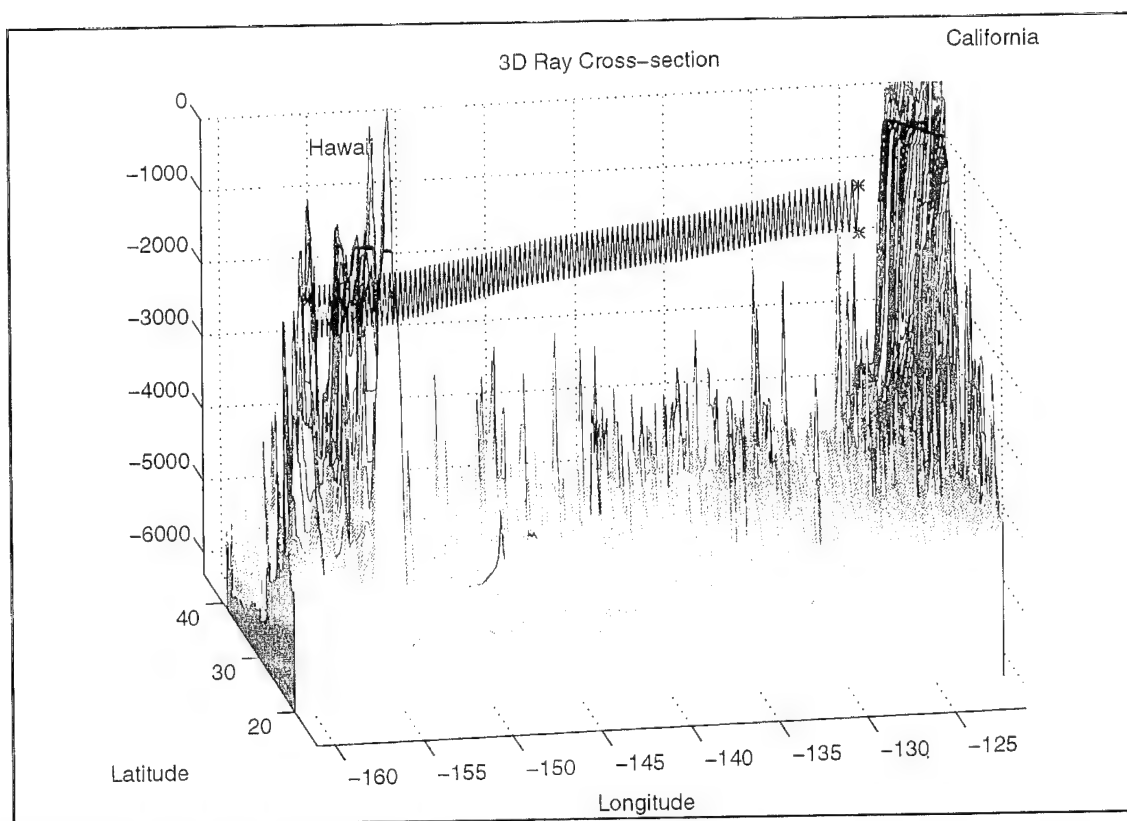

Figure 8. A three-dimensional view of the bathymetry. Source and receiver locations are superimposed on the figure as well as a near-axial raypath.

17

2.   Temporal Variability

In Figure 9 the standard deviation of sound speed in a vertical slice along the transmission path, calculated from the POCM for the two year period of this study, is shown. A region of increased variability which appears to be associated with mesoscale phenomenon lies just beyond the 1500 km range and seems to correspond to the average position of the subtropical front.   Again note the zone of decreased variability below approximately 500 m.

C.   RAYPATH ANALYSIS

As indicated in Chapter 1, the examination of three acoustic issues were the thrust of this simulation analysis: reliability, stability and travel time variability.

1.   Acoustic Reliability

Rays were traced for a single azimuth in a vertical fan for launch angles between -15° (downward) and +15° (upward) per six-day time step.   Out of these rays an average of 110 eigenrays per time slice were found for the deep receiver and 131 eigenrays were found for the axial receiver.   The reduced number of eigenrays for the deep receiver is expected due to its decreased proximity to the sound channel axis.

Figure 10 presents a typical vertical geometry of a near-axial raypath.   Generally the width of the vertical envelope for shallow-angled rays is no more than 300-400 m and, more importantly, the depth of the ray trajectory remains well below the area of greatest variability in the water column

18
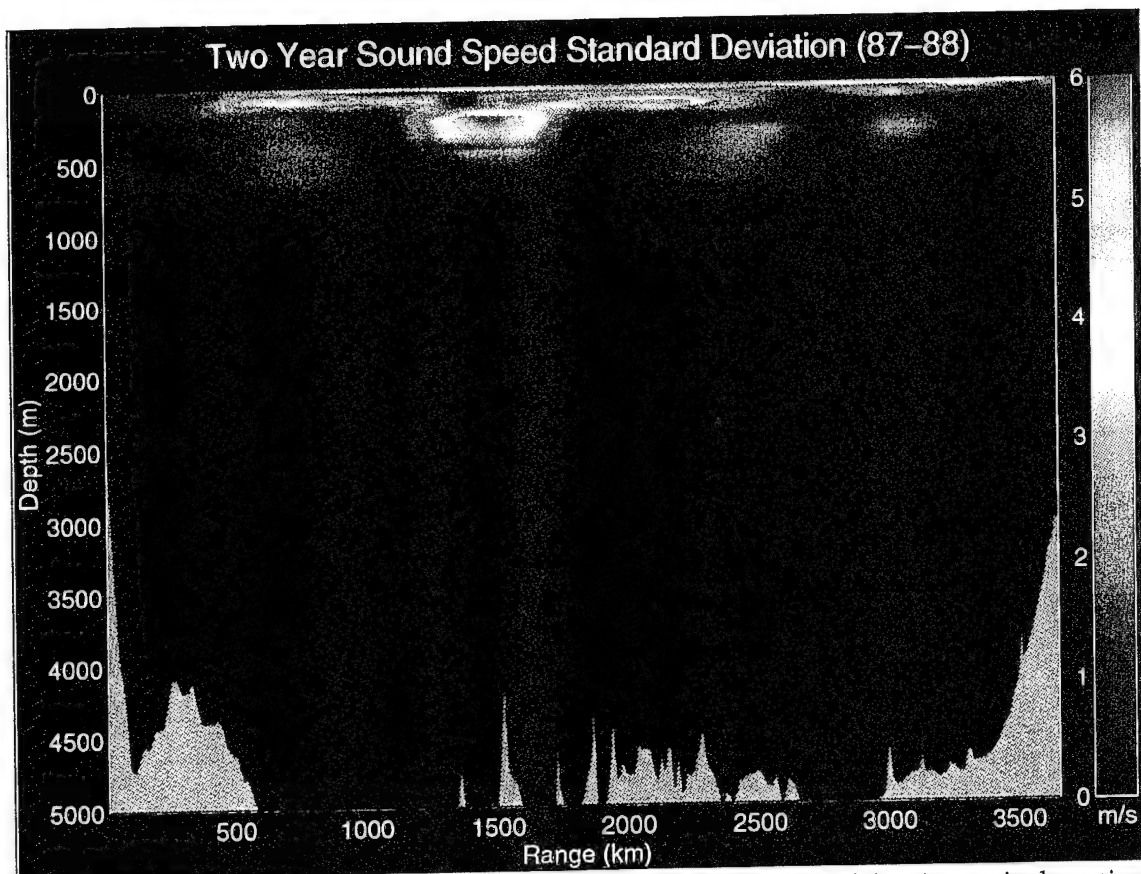
Figure 9. Standard deviation of sound speed in a Hawaii-to-California vertical section over a two-year time period.
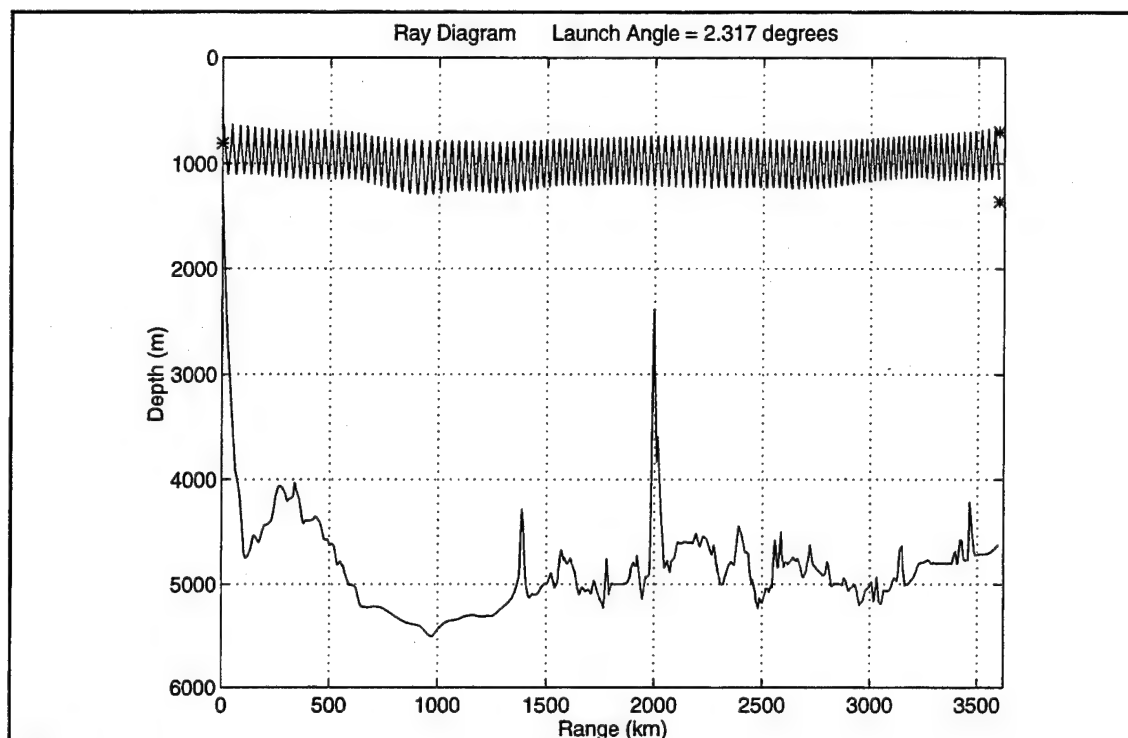
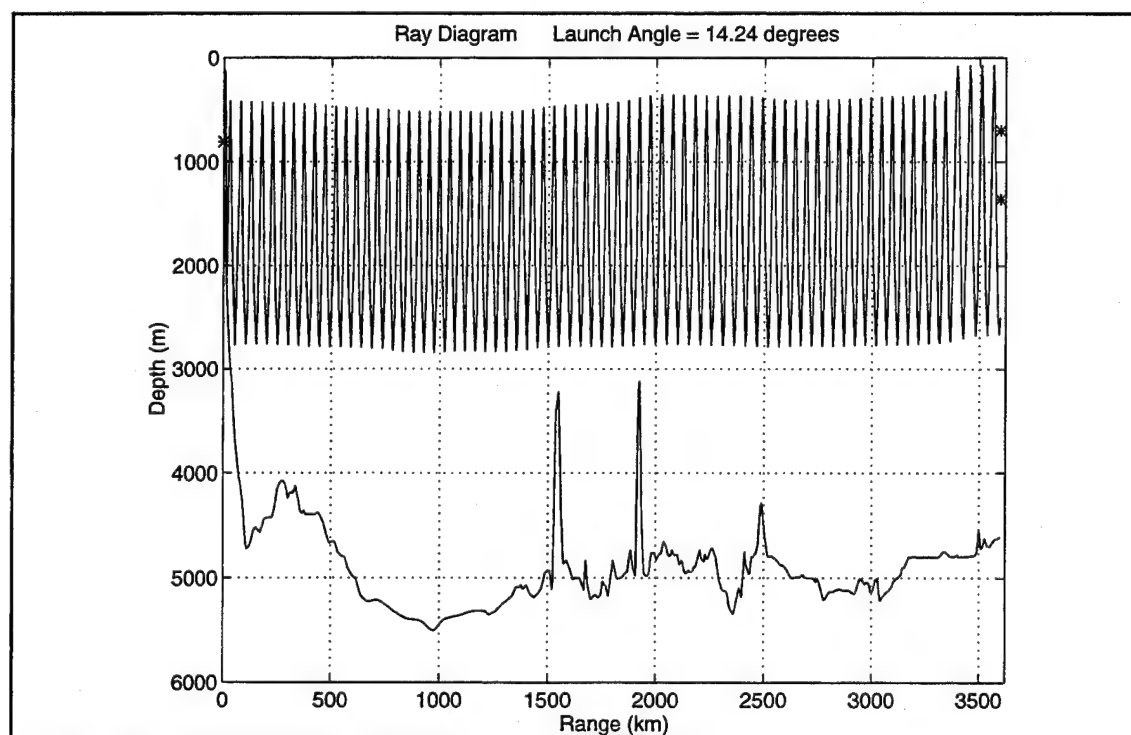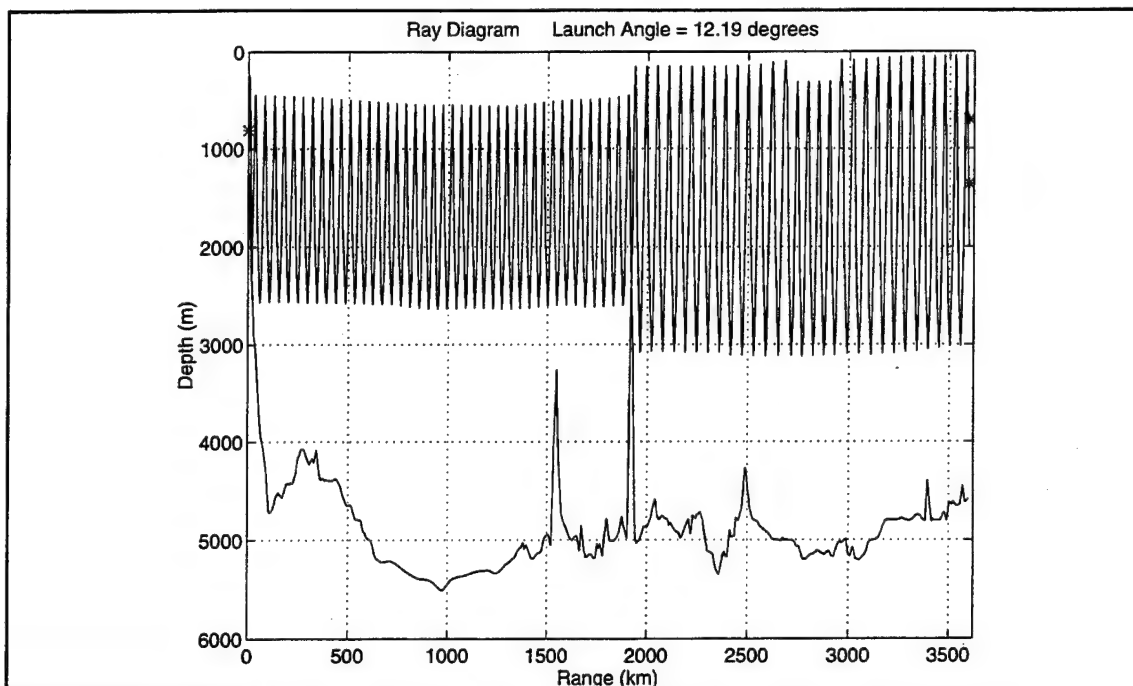**Figure 10.** Vertical path geometry of a near-axial ray.

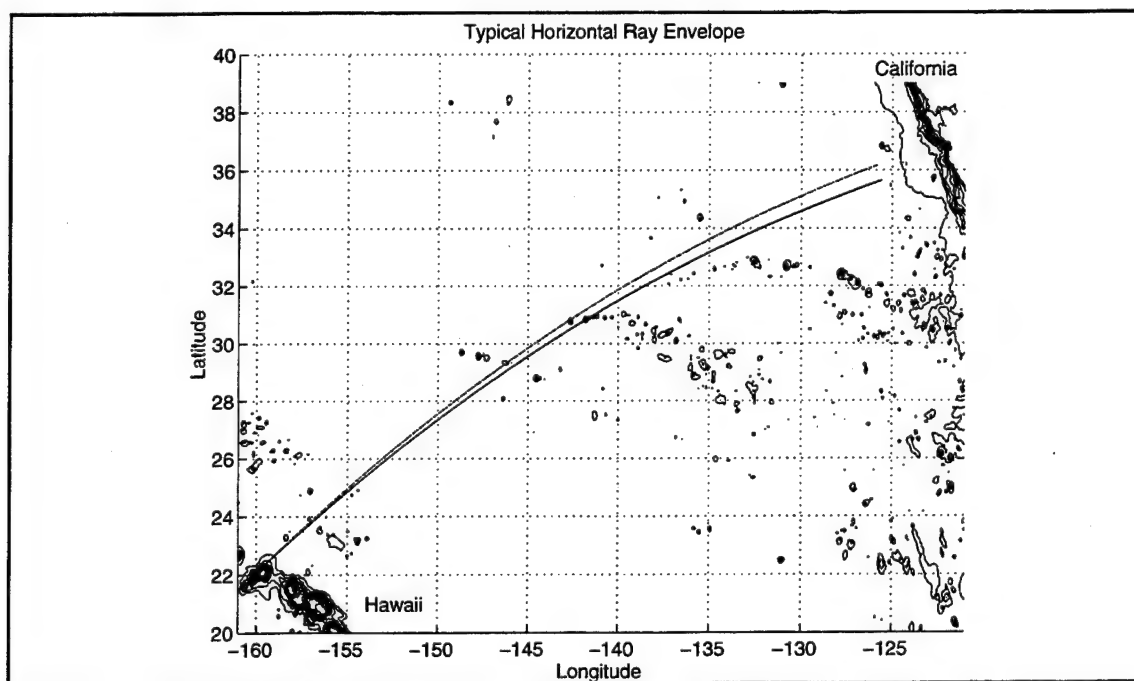**Figure 11.** Vertical path geometry of a deep-cycling ray.

20

(see Figure 9).

A typical deep cycling ray path is shown in Figure 11. The width of the vertical envelope is far greater than the near axial, increasing to over 2000 m. It is important to note that the upper turning points are located within the region of high variability within the water column.

Figure 12 shows a vertical geometry of a deep-cycling ray that has been impacted by one of the Moonless Mountains. Depending on the angle of incidence on the seamount, some rays could be reflected into much steeper paths that have numerous surface and bottom interactions. These significant boundary interactions and losses would render them unreliable. However, some other impacted rays, such as the one shown in Figure 12, were merely reflected into slightly steeper paths that do not encounter further boundary interactions beyond the seamount. These mild alterations in ray trajectories were rare in occurrence and only affected ray launch elevation angles of magnitude 12° and higher.

Horizontal refraction is considerable. Figure 13 displays the horizontal path geometry of both a near-axial (southern ray) and a steep raypath (northern ray) along with contoured topography. Both rays were launched with the same azimuth angle. Refractive effects are obvious as steeper ray paths are influenced more by the north-south temperature gradient, refracting northward toward cooler temperatures (and lower sound speeds). A great circle path with an initial

21

Figure 12. Vertical path geometry of a steep ray with bathymetry interaction.

Figure 13. Horizontal path geometry of a deep-cycling (upper curve) and a near-axial ray (lower curve), both having the same initial azimuth angle. The horizontal path geometry of the near-axial ray coincides with the great circle path.

22

azimuth angle of 58.1° (same initial azimuth as traced rays) is also shown and appears concurrent with the near-axial ray path. Horizontal separations between near-axial paths and deep-cycling paths launched with the same azimuthal angle off Hawaii can be as much as 100 km near California.

In addition to the effect of the topography in the Murray Fracture Zone, interaction with the bottom near the source in Hawaii is also observed. Figure 14 shows a dot plot of travel time versus vertical launch angle with a receiver depth of 700 m for all eigenrays calculated over the two-year study period. The general shape of decreasing arrival time with increasing magnitude of angle is expected as steeper rays travel through higher sound speeds and thus arrive sooner. However, two anomalies exist, one between -7° and -10° and the other one between +8° and +10°. Rays launched at these two angular ranges strike the sloping bottom near Hawaii and are reflected out into more axial paths, causing the corresponding travel times to increase as slower sound speeds are encountered. Similar features can be seen in Figure 15 for the 1359-m receiver. The lack of near-axial arrivals is apparent for the deeper receiver, which is located over 500 m below the sound channel axis.

2. Arrival Structure Stability

The simulated time series of arrival structures provides a means for analyzing both stability and travel time variability. First we look at stability.

23
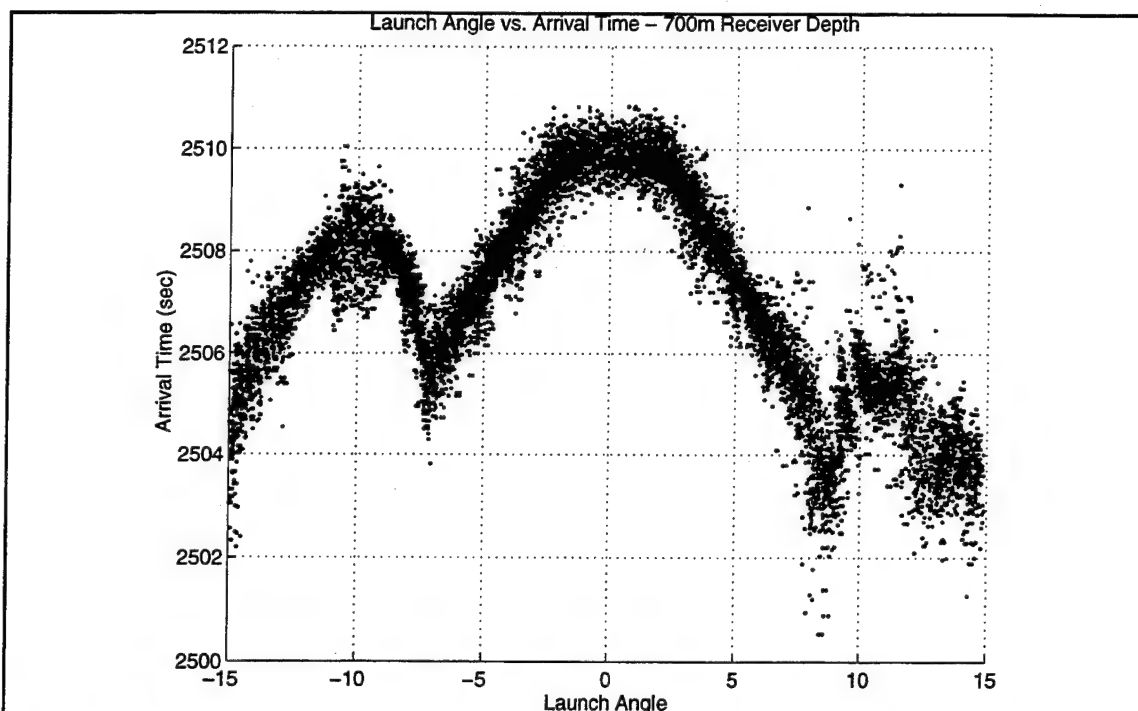
Figure 14. Dot plot of travel time versus vertical launch angle with a receiver depth of 700 m for all eigenrays calculated over a two-year study period.
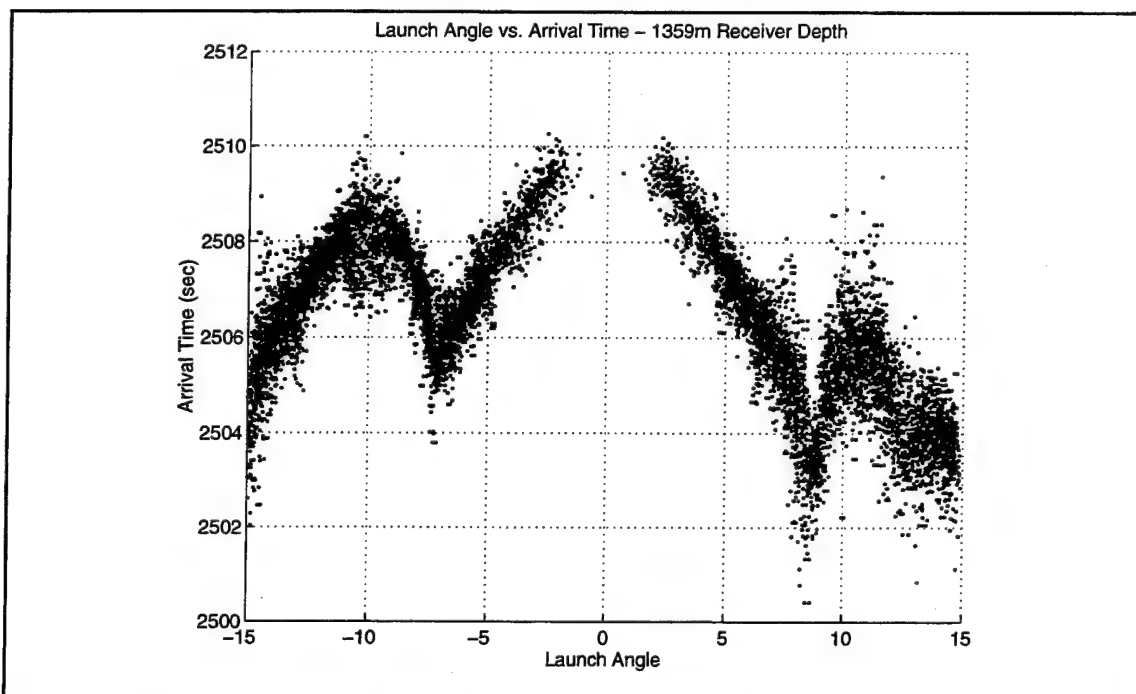
Figure 15. Dot plot of travel time versus vertical launch angle with a receiver depth of 1359 m for all eigenrays calculated over a two-year study period.

24

The ATOC sound source is planned to transmit a phase-modulated signal at a carrier frequency of 75 Hz. The modulation is an m-sequence of 1023 digits, with each digit containing two cycles. This gives a total sequence period of:

$$T = \frac{1}{75\ Hz} * 1023\ digits * \frac{2\ cycles}{digit} = 27.28\ seconds$$

The duration of the multipath arrival structure will last approximately eight seconds, so the entire arrival structure will be observed without lane ambiguity. The matched filter output is effectively a pulse having a duration of 26.6667 ms, but in generating a simulated arrival structure the pulse length was roughly doubled in an attempt to account for dispersion effects.

The arrival structure was determined from the arrival time, amplitude and phase shift associated with each eigenray. Typical simulated arrival structures for the 700-m receiver and the 1359-m receiver are shown in Figures 16 and 17, respectively. Amplitudes ramp up to peak at later arrival times for the 700-m receiver, signifying the strength of the more dominant axial eigenrays. The arrival structure for the 1359-m receiver noticeably lacks the higher amplitude later arrivals and has a less banded pattern than the 700-m receiver. Already we can see the effect of receiver depth on
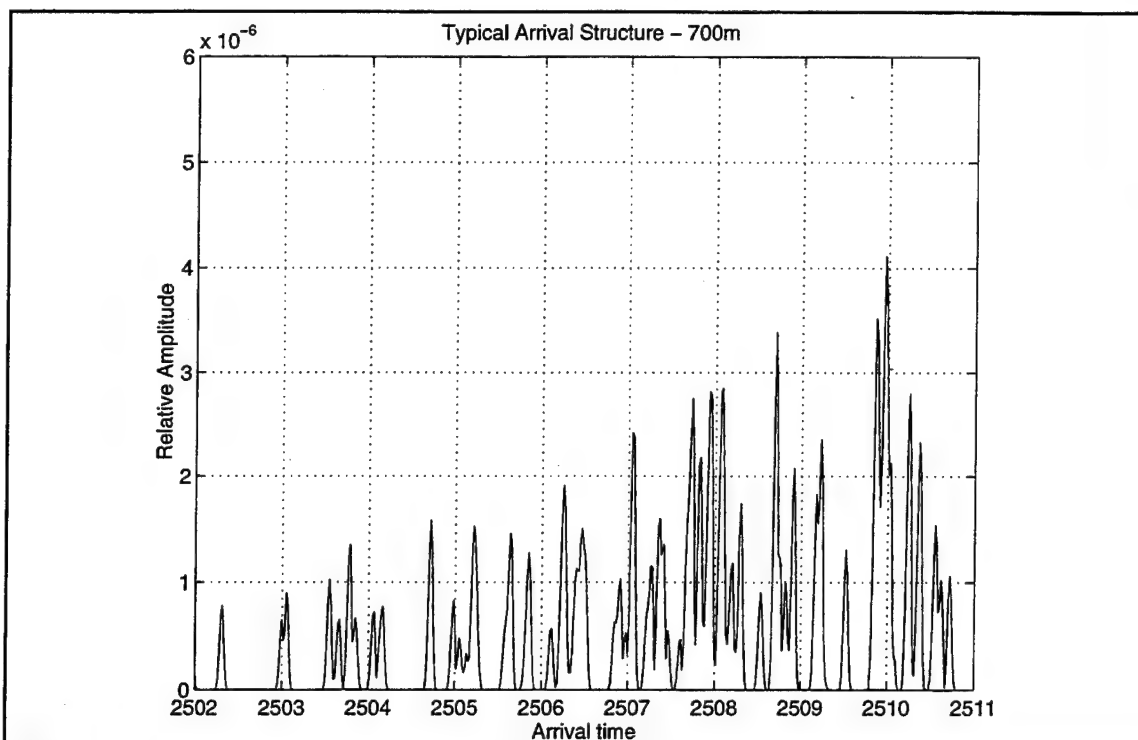
25

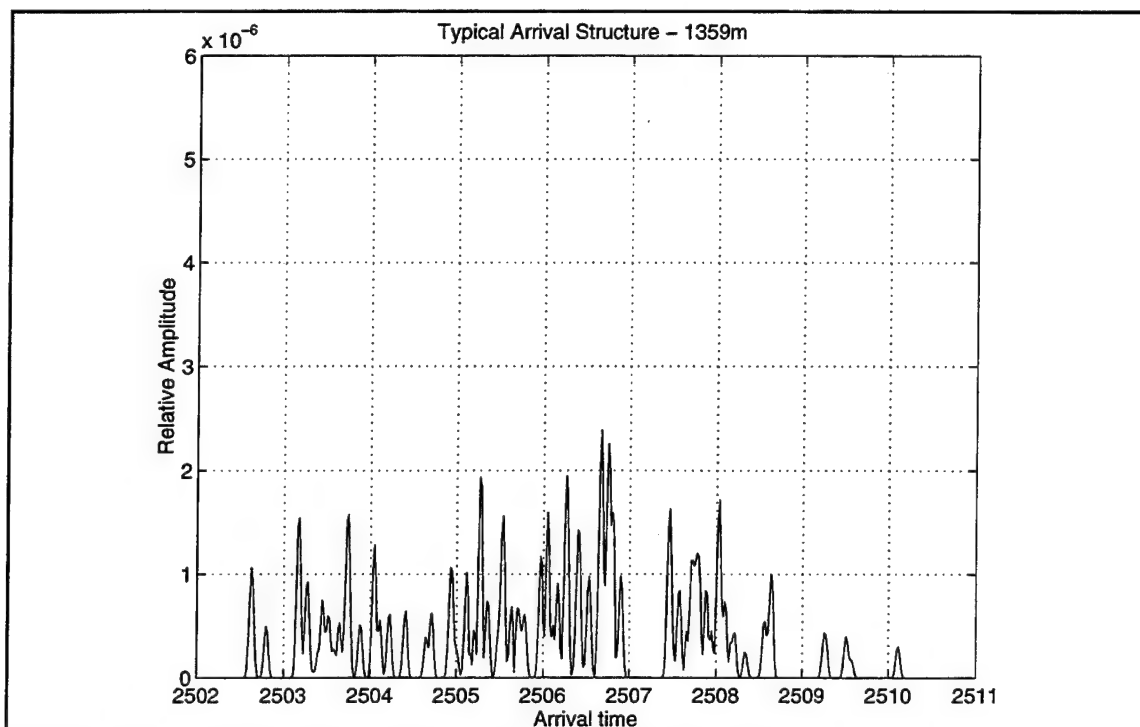**Figure 16.** Typical arrival structure for the 700-m receiver.
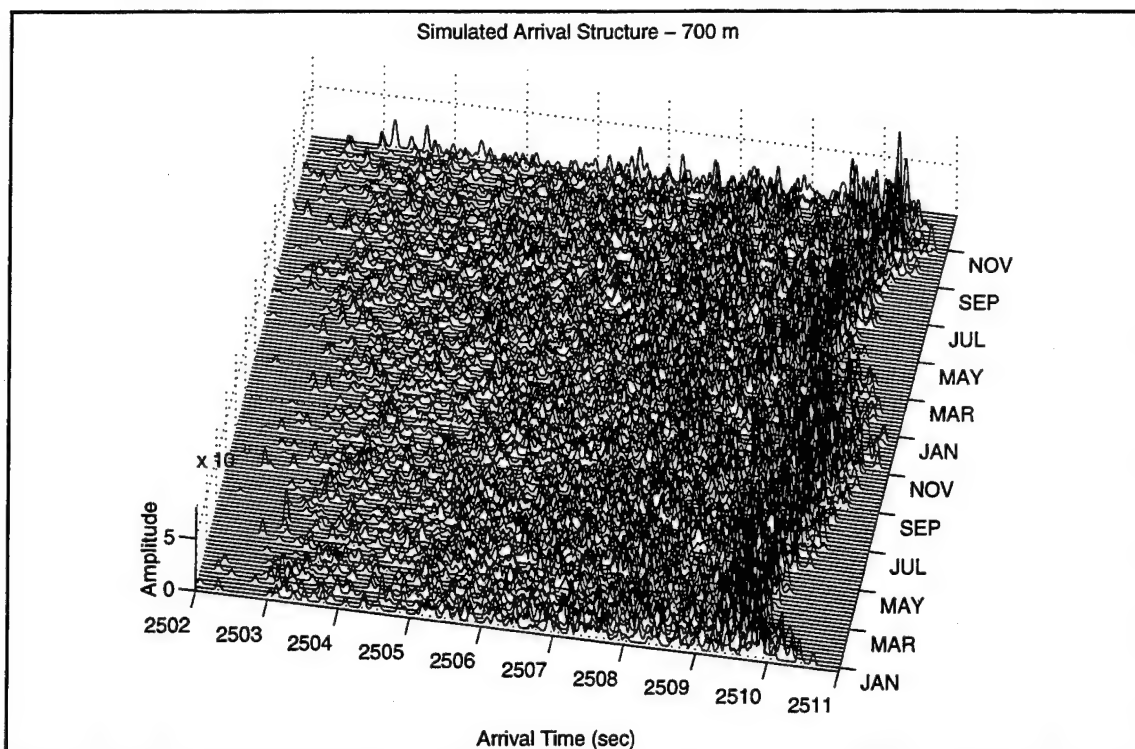

Figure 17. Typical arrival structure for the 1359-m receiver.

26

arrival structure, as the upper turning points of steeper eigenrays pick up more of the natural variability of the upper water column, resulting in a less organized arrival structure.

Arrival structures were computed for each six-day "snapshot" for both the 700 m and 1359 m receiver depths. The two time series are shown in waterfall plots displayed in Figures 18 and 19, respectively. In viewing the arrival structure for the deep (1359 m) receiver it is difficult to "visualize" stable patterns of arrivals or any correlation over the two year period. A seasonal pattern is evident for the near-axial (700 m) receiver, especially among the later (and more axial) arrivals. Except for this limited band, it is similarly difficult to "visually" track distinct patterns of arrivals over geophysical time.

The correlations and the lag times of the correlation peaks between the first arrival pattern and all the later arrival patterns for each receiver depth were calculated. The results as shown in Figure 20(a) for the deep receiver indicate a consistent 0.6 correlation, which is perhaps higher than one would expect from a visual inspection of the waterfall plots. In addition, time shifts from zero lag are plotted, showing a pronounced mesoscale oscillation and a less defined seasonal oscillation. Rms lag time variability for the deep receiver is estimated to be 0.51 s.
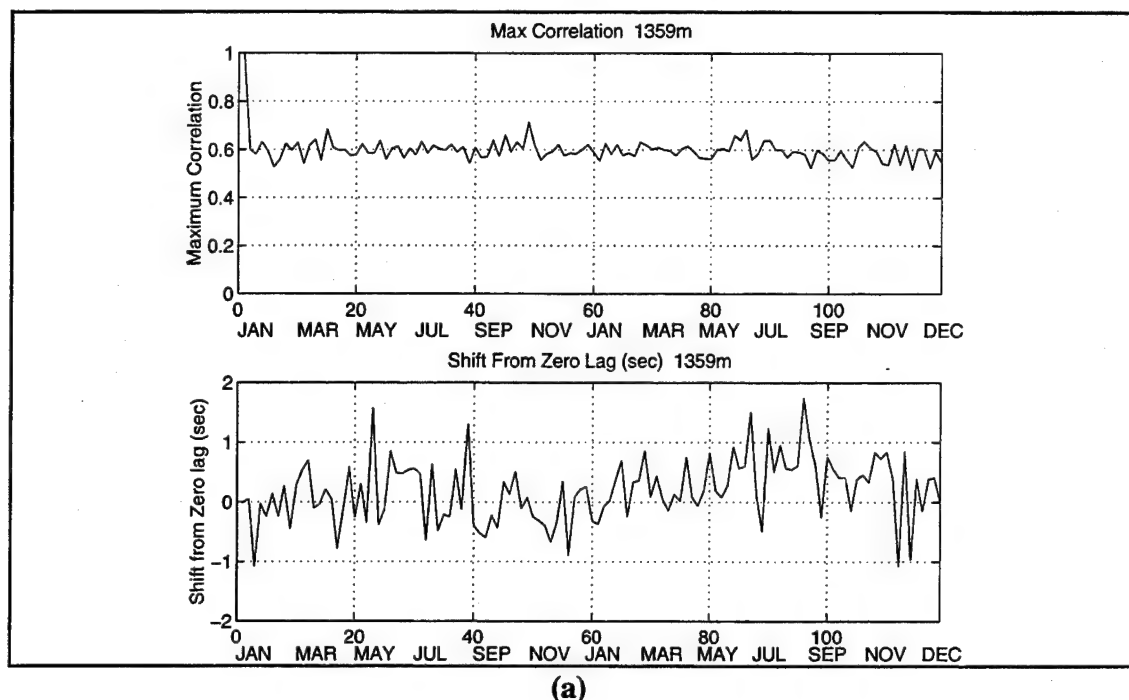
Figure 20(b) displays results for the near-axial receiver, yielding a 0.6 correlation also. In contrast to the
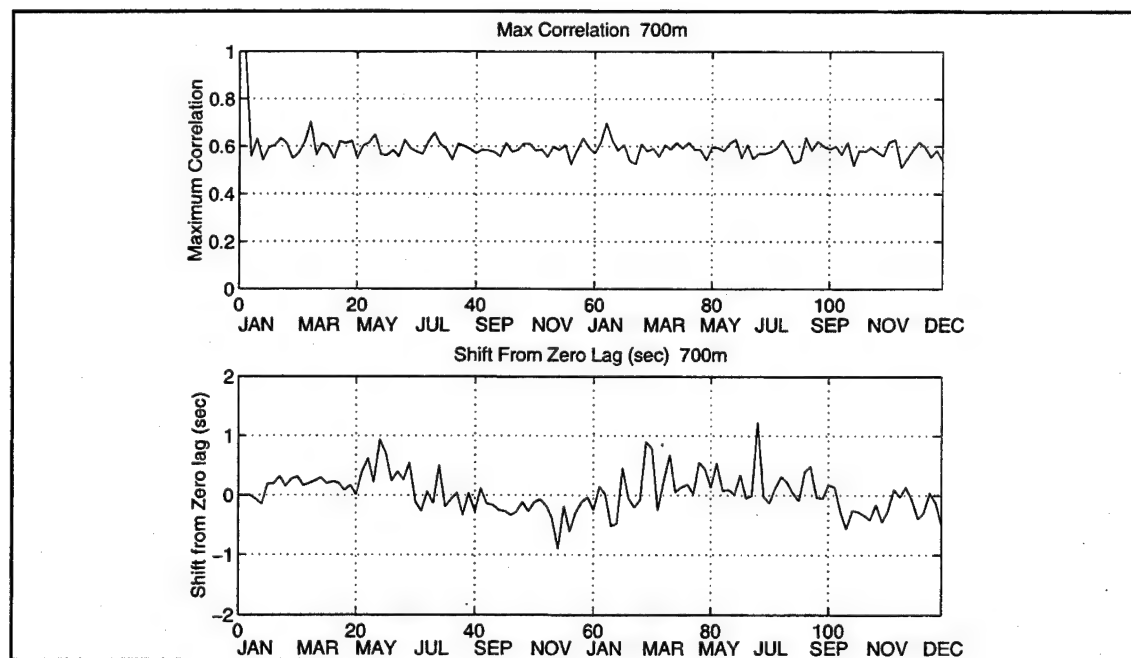
27

Figure 18. Arrival structures over two year time period for the 700-m receiver depth.
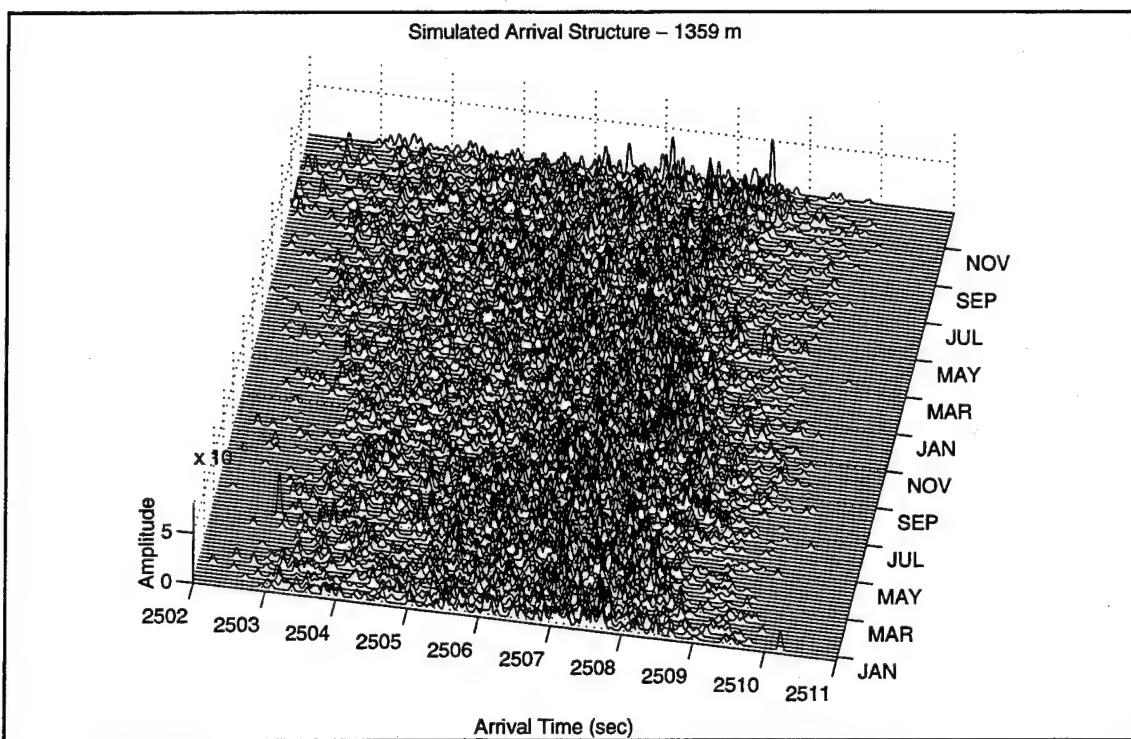
Figure 19. Arrival structures over two year time period for the 1359-m receiver depth.

28

Figure 20. Correlation coefficients and the lag times of the correlation peaks between the reference (first) arrival pattern and all the later arrival patterns for (a) a receiver depth of 1359 m and (b) a receiver depth of 700 m.

29

deep receiver lag time plot, seasonal oscillations are very pronounced and mesoscale oscillations are very subdued. Rms lag time variability for the near-axial receiver is estimated to be 0.33 s.

In order to facilitate visual tracking of arrivals in the waterfall plots, correlation lag times were subtracted from their respective arrival structures and the results are plotted in Figures 21 and 22. Obvious bands of consistent arrivals can be seen for both receiver depths, indicating a certain degree of stability over time and also identifying which arrivals are the most stable.

3. Travel Time Variability

To characterize and quantify travel time variability over the entire two-year time period, the shift from zero lag times were taken as time series and spectral analysis done for each receiver depth. Figure 23 shows a comparison of the relative spectra between the near-axial and deep receiver depths. Note frequency is plotted in cycles/year. The dominant frequency for both depths is seasonal (one cycle/year) at roughly similar values for each, but mesoscale frequencies are clearly more significant at the deeper receiver.

To reinforce the results of the lag time analysis, individual eigenrays were selected for similar analysis. Two reasonably stable eigenrays were isolated, one near-axial at 5° and the other steep at 13°. Figure 24 shows the comparison of the relative spectra. For the near-axial eigenray, the
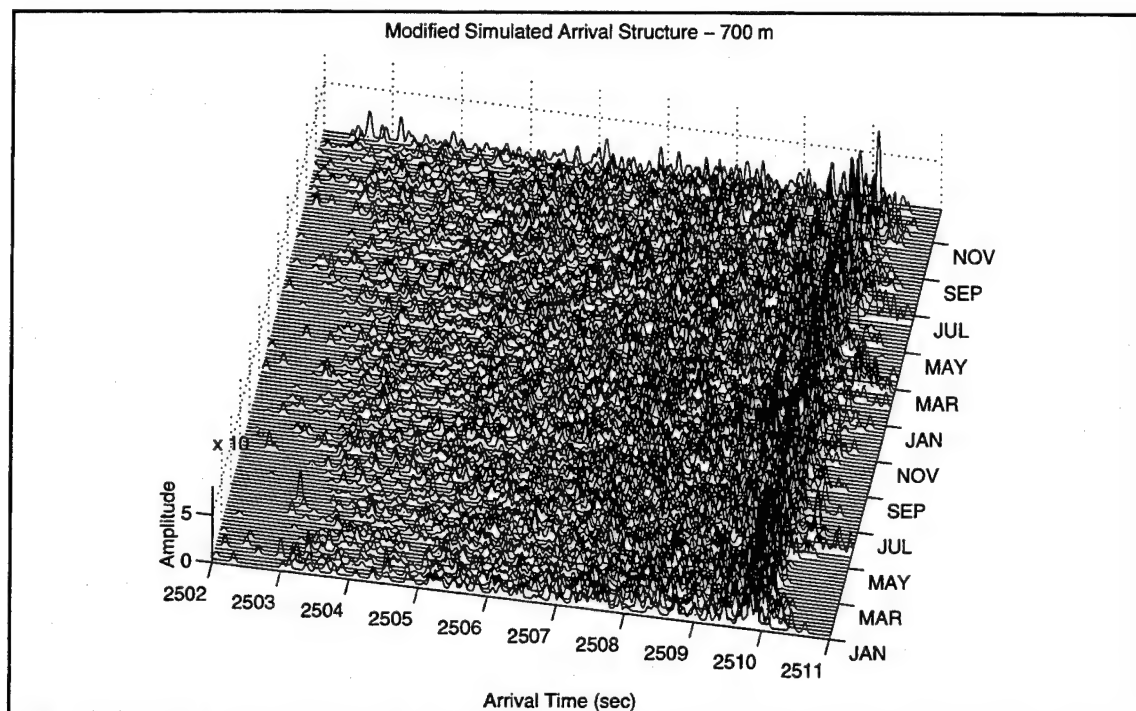
Figure 21. Aligned 700-m arrival structures with correlation lag times subtracted resulting in an improved visualization of stable arrivals.
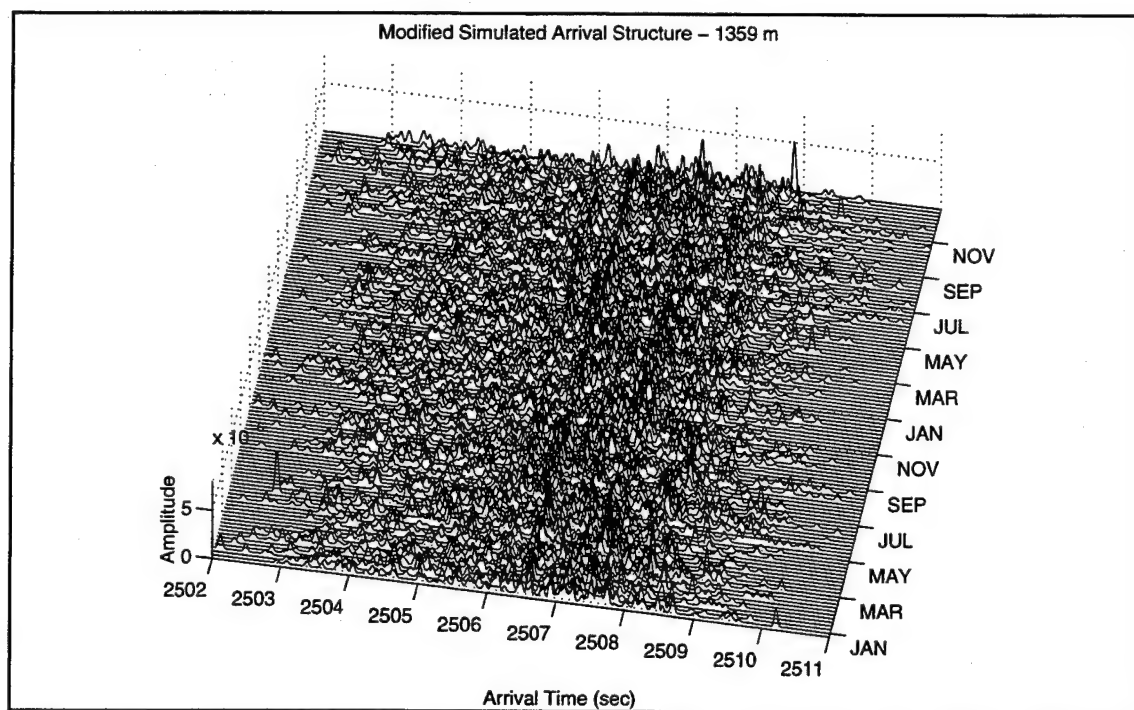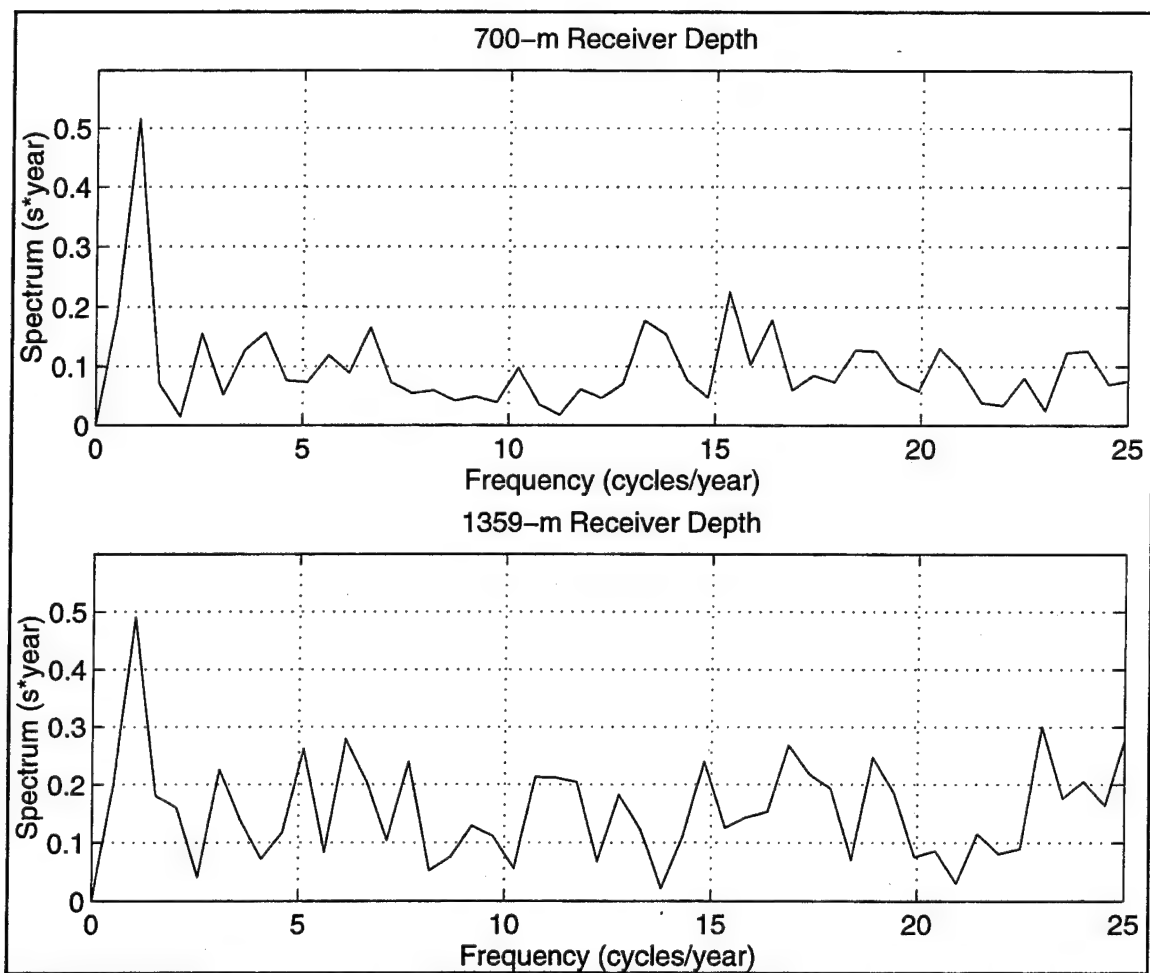

Figure 22. Aligned 1359-m arrival structures with correlation lag times subtracted resulting in an improved visualization of stable arrivals.

Figure 23. Frequency spectra of time series of the correlation peak lag times for receiver depths of 700 m (upper panel) and 1359 m (lower panel).
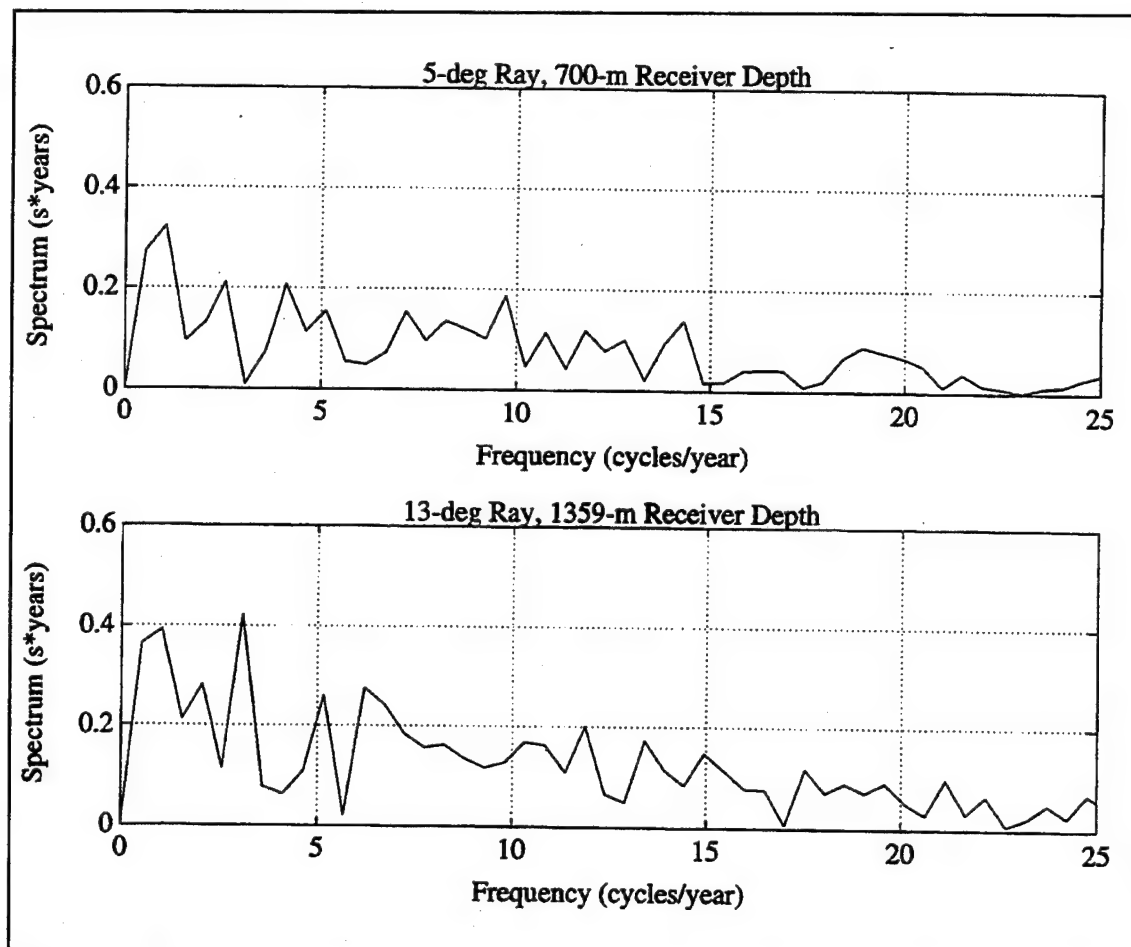
Figure 24. Frequency spectra of time series of travel times for a near-axial eigenray (upper panel) and a deep-cycling eigenray (lower panel).

dominant frequency is seasonal, while for the steep eigenray seasonal and mesoscale variability appear nearly equal in size. The distinct peak at three cycles/year is interesting in that it could be an indication of "sensitivity" to a particular scale of mesoscale phenomenon. This "sensitivity" might be inherent to the particular eigenray selected for analysis, and other eigenrays may be responsive to other corresponding scales of variability.

The overall rms travel time variability, or "geophysical noise", is estimated to be approximately 0.28 s for near-axial rays and 0.42 s for steep rays. These estimates are consistent with the lag time values presented in the previous subsection of 0.33 s and 0.51 s for the near-axial and deep receivers, respectively. The frequency spectra indicate that travel time changes for near-axial rays are primarily due to seasonal changes, while for steep rays a combination of seasonal and mesoscale changes contribute to the overall variability of travel time.

IV. CONCLUSIONS

In this thesis research, a planned ATOC transmission from Hawaii to Monterey was simulated for a two-year period using a ray-based acoustic model and a global ocean circulation model. The simulated raypath geometries, arrival structures, and the effects of mesoscale, gyre and seasonal variability were analyzed.

Major conclusions based on this study are as follows:

1. Multipath arrival structure strongly dependent on receiver depth.

2. Multipath arrival structure quasi-stable with a correlation of 0.6 between arrival patterns at different times.

3. It is difficult to "visually" track individual arrivals over time without additional alignment. However, the temporal change of the time lag of correlations peaks is consistent with individual ray travel-time variations.

4. Subtraction of correlation peak times allows for alignment to facilitate visual tracking of individual arrivals.

5. Bottom topography in the vicinity of the Moonless Mountains has an occasional mild effect on rays with launch angles larger than approximately 12˚.

35

6. Travel time variability ("noise") estimates are 0.42 seconds rms for steep rays and 0.28 seconds rms for near-axial rays.

7. Near-axial ray variability is due primarily to seasonal changes, while steep ray variability is due to a combination of seasonal and mesoscale changes.

8. A longer duration simulation study is needed to appropriately characterize "noise" due to inter-annual cycles.

LIST OF REFERENCES

Cartwright, D.E., "Preliminary Estimates of Tidal Variations Along ATOC Transmission Paths," *ATOC occasional Notes,* Number 3, 1993.

Chiu, C-S., A.J. Semtner, C.M. Ort, J.H. Miller and L.L. Ehret, "A Ray Variability Analysis of Sound Transmission from Heard Island to California," *The Journal of the Acoustical Society of America,* Vol. 96:4, pp. 2380-2388, 1994.

Chiu, C-S., Department of Oceanography, Naval Postgraduate School, Monterey, CA, Personal Communication, 1995.

Jones, R.M., J.P. Riley and T.M. Georges, "HARPO: A Versatile Three-Dimensional Hamiltonian Ray Tracing Program for Acoustic Waves in an Ocean with Irregular Bottom," Wave Propagation Laboratory, National Oceanic and Atmospheric Administration, Boulder, CO, 457 pp., 1986.

Mackenzie, K.V. "Nine-term Equation for Sound Speed in the Ocean," *Journal of the Acoustical Society of America,* Vol. 70:4, pp. 807-812, 1981.

Menard, H.W., "Marine Geology of the Pacific," McGraw-Hill, Inc., New York, 1964.

Munk, W.H., and A.M.G. Forbes, "Global Acoustic Warming: An Acoustic Measure?," *Journal of Physical Oceanography,* Vol. 19, pp. 1765-1778, 1989.

Newhall, A.E., J.F. Lynch, C-S. Chiu, and J.R. Daugherty, "Improvements in Three Dimensional Ray Tracing Codes for Underwater Acoustics," *Computational Acoustics: Ocean Acoustic Models and Supercomputing,* North-Holland, Amsterdam, 1990.

Pickard, G.L., and W.J. Emery, "Descriptive Physical Oceanography," Pergamon Press, 1990.

Semtner, A.J., and R.M. Chervin, "A Simulation of the Global Ocean Circulation with Resolved Eddies," *Journal of Geophysical Research*, Vol. 93:C12, pp. 15502-15522 and 15767-15775, 1988.

Semtner, A.J., and R.M. Chervin, "Ocean General Circulation from a Global Eddy Resolving Ocean Model," *Journal of Geophysical Research,* Vol. 97:C4, pp. 5493-5550, 1992.

Semtner, A.J., "Very High-resolution Estimates of Global Ocean Circulation, Suitable For Carbon-cycle Modeling," *Proceedings of the Snowmass Global Change Institute on the Global Carbon Cycle,* Office of Interdisciplinary Earth Studies, Boulder, in press, 1995.

INITIAL DISTRIBUTION LIST

1. Defense Technical Information Center   2
    Cameron Station
    Alexandria, VA 22304-6145

2. Library, Code 52   2
    Naval Postgraduate School
    Monterey, CA 93943-5101

3. Dr. Robert H. Bourke (Code OC/BO)   1
    Department of Oceanography
    Naval Postgraduate School
    Monterey, CA 93943-5000

4. Dr. Ching-Sang Chiu (Code OC/CI)   1
    Department of Oceanography
    Naval Postgraduate School
    Monterey, CA 93943-5000

5. Dr. Albert J. Semtner (Code OC/SE)   1
    Department of Oceanography
    Naval Postgraduate School
    Monterey, CA 93943-5000

6. LT Robert A. Staten, USN   1
    598 B Michelson Road
    Monterey, CA 93940

7. Director, Naval Oceanography Division   1
    Naval Observatory
    34th and Massachusettes Avenue NW
    Washington, DC 20390

8. Commander   1
    Naval Oceanographic Command
    Stennis Space Ctr
    Bay St. Louis, MS 39539-5000

9. ATOC Project Office   1
    Scripps Institution of Oceanography
    9500 Gilman Drive, 0225
    La Jolla, CA 92093-0225